Design and analysis of a broadband dispersion compensating photonic crystal fiber Raman amplifier operating in S-band

Shailendra K. Varshney, Takeshi Fujisawa, Kunimasa Saitoh, and Masanori Koshiba

Division of Media and Network Technologies, Hokkaido University, Sapporo 060-0814, Japan
skvarshney_10@yahoo.co.uk

Abstract: This paper presents an optimized design of a dispersion compensating photonic crystal fiber (PCF) to achieve gain-flattened Raman performances over S-band using a single pump. Genetic algorithm interfaced with an efficient full-vectorial finite element modal solver based on curvilinear edge/nodal elements is used as an optimization tool for an accurate determination of PCF design parameters. The designed PCF shows high negative dispersion coefficient (–264 ps/nm/km to –1410 ps/nm/km) and negative dispersion slope, providing coarse dispersion compensation over the entire S-band. The module comprised of 1.45-km long optimized PCF exhibits ±0.46 dB gain ripples over 50 nm wide bandwidth and shows a very low double Rayleigh backscattering value (–59.8 dB). The proposed module can compensate for the dispersion accumulated in one span (80-km) of standard single mode fiber with a residual dispersion of ±700 ps/nm, ensuring its applicability for 10 Gb/s WDM networks. Additionally, the designed PCF remains single mode over the range of operating wavelengths.

OCIS codes: Fiber design and fabrication (060.2280); (999.9999) Photonic crystal fiber

References and Links

1. S. Namiki, Y. Ikegami, Y Shirasaka, and I. Oh-ishi, "Highly coupled high power pump laser modules," *in Proc. Optical Amplifiers and Their Application (OAA 1993)*, Paper MD5, (1993).
2. M. N. Islam, *Raman Amplification for Telecommunications 1 and 2* (Springer-Verlag, New York, 2004).
3. C. Headly and G. P. Agarwal, *Raman Amplification in Fiber Optical Communication Systems* (Academic Press, New York, 2004).
4. J. Bromage, "Raman amplification for fiber communication systems," J. Lightwave Technol. **22**, 79-93 (2004).
5. K. Thyagarajan and C. Kakkar, "Novel fiber design for flat gain Raman amplification using single pump and dispersion compensation in S-band," J. Lightwave Technol. **22**, 2279-2286 (2004).
6. Z. Yusoff, J.H. Lee, W. Belardi, T.M.Monro, P.C. Teh, and D. J. Richardson, "Raman effects in a highly nonlinear holey fiber: amplification and modulation," Opt. Lett. **27**, 424-426 (2002).
7. C.J.S. de Matos, K. P. Hansen, and J. R. Taylor, "Experimental characterization of Raman gain efficiency of holey fiber," Electron. Lett. **39**, 424-425 (2003).
8. M. Bottacini, F. Poli, A. Cucinotta, and S. Selleri, "Modeling of photonic crystal fiber Raman amplifiers," J. Lightwave Technol. **22**, 1707-1713 (2004).
9. S.K. Varshney, K. Saitoh, and M. Koshiba, "Raman performances of ultralow loss photonic crystal fiber amplifiers", *in Proc. Lasers and Electro-Optics (IQEC/CLEO-PR 2005)*, paper no. CWE2-3, (2005).
10. S.K. Varshney, K. Saitoh, and M. Koshiba, "A novel design of dispersion compensating photonic crystal fiber Raman amplifier," IEEE Photon. Technol. Lett. **17**, 2062-2064 (2005).
11. S.K. Varshney, T. Fujisawa, K. Saitoh, and M. Koshiba, "Novel design of inherently gain-flattened discrete highly nonlinear photonic crystal fiber Raman amplifier and dispersion compensation using a single pump in C-band," Opt. Express **13**, 9516-9526 (2005). http://oe.osa.org/abstract.cfm?id=86238
12. S.K. Varshney, K. Saitoh, T. Fujisawa, and M. Koshiba, "Design of gain-flattened highly nonlinear photonic crystal fiber Raman amplifier using a single pump: a leakage approach," *in Proc. Optical Fiber Communication (OFC/NFOEC)*, paper no. OWD4, (2006).
13. T.A. Birks, J.C. Knight, and P.St.J. Russell, "Endlessly single-mode photonic crystal fiber," Opt. Lett. **22**, 961-963 (1997).
14. A. Bjarklev, J. Broeng, and A.S. Bjarklev, *Photonic Crystal Fibres*, (Kulwer Academic Publishers 2003).

15. T. Fujisawa, K. Saitoh, K. Wada, and M. Koshiba, "Chromatic dispersion profile optimization of dual-concentric-core photonic crystal fibers for broadband dispersion compensation," Opt. Express **14**, 893-900 (2006). http://oe.osa.org/abstract.cfm?id=87588
16. K. Saitoh and M. Koshiba, "Full-vectorial imaginary-distance beam propagation method based on a finite element scheme: application to photonic crystal fibers," IEEE J. Quantum Electron. **38**, 927-933 (2002).
17. M. Koshiba and K. Saitoh, "Applicability of classical optical fiber theories to holey fibers," Opt. Lett. **29**, 1739-1741 (2004).
18. J. Bromage, K. Rottwitt, and M. E. Lines, "A method to predict the Raman gain spectra of germanosilicate fibers with arbitrary index profiles," IEEE Photon. Technol. Lett. **14**, 24-26 (2002).
19. L. Farr, J. C. Knight, B. J. Mangan, and P. J. Roberts, "Low loss photonic crystal fiber," *in Proc. European Conference on Optical Communications* (*ECOC 2002)*, paper PD 1.3, (2002).
20. K. Tajima J. Zhou, K. Nakajima, and K. Sato "Ultralow loss and long length photonic crystal fiber," J. Lightwave Technol. **22**, 7-9 (2004).
21. B.J. Mangan, F. Couny, L. Farr, A. Langford, P.J. Roberts et al., "Slope-matched dispersion-compensating photonic crystal fiber," *in Proc. Lasers and Electro-Optics (CLEO 2004)*, pp. 1069-1070, (2004).
22. P.J. Roberts, B.J. Mangan, H. Sabert, F. Couny, T.A. Birks, J.C. Knight, and P.St. J. Russell, "Control of dispersion in photonic crystal fibers," J. Opt. Fiber. Commun. Rep. **2**, 435-461 (2005).
23. S.G. Leon-Saval, T.A. Birks, N.Y. Joy, A.K. George, W.J. Wadsworth, G. Kakarantzas, and P.St.J. Russell, "Splice-free interfacing of photonic crystal fibers," Opt. Lett. **30**, 1629-1634 (2005).

1. Introduction

An interest has been revived in silica based fiber Raman amplifiers (FRAs) after the successive development and commercialized availability of high powered laser diodes [1-4]. Raman amplification based on stimulated Raman scattering process has been one of the key optical amplifier technologies to upgrade the transmission bandwidth of the wavelength division multiplexed (WDM) networks due to their capabilities in terms of reduced noise performance and decreased nonlinear penalties. This is because the spectral region where significant Raman gain occurs depends primarily on pump wavelength and power. Therefore, amplification of discrete or lumped and distributed FRA can be achieved in any transmission band. Moreover, discrete Raman amplification can efficiently be integrated with the dispersion compensation. Hence, Raman amplification can permit wide bandwidth and long reach simultaneously [2].

The attenuation in the S-band is comparable to or better than attenuation in the L-band, and channels in S-band are far less sensitive to micro- and macro-bending losses. In addition, dispersion of standard single mode fiber (SSMF) in the S-band is also lower than dispersion in the longer wavelength bands. Therefore, Raman amplification can be a viable approach to achieve sufficient amplification in S-band, extending the bandwidth [2] in compare to existing EDFA technology which doesn't provide the amplification over S-band. Raman amplification over S-band in W-type conventional optical fiber was obtained [5] by a single pump, where the fiber shows negative dispersion coefficient (–380 ps/nm/km to –515 ps/nm/km) over 32 nm bandwidth (1480-1511 nm).

On the other hand, photonic crystal fibers, thin pure silica strands with parallel running microscopic sized air-holes in the cladding, have attracted attention to potentially act as Raman amplifiers [6-12]. The strong wavelength dependent cladding index imparts novel properties such as endlessly single mode regime [13], large or small effective mode area, high nonlinearity, and overall manageable dispersion properties [14]. The precise control of air-hole diameter-d and lattice constant-Λ facilitates small modal effective area and high negative dispersion characteristics, giving rise to higher Raman gain efficiency (RGE). It is to be noticed that high RGE values can be obtained for pure silica core PCFs rather than doping its core like in conventional optical fibers. Raman amplification in S-band using PCFs has not been reported so far. Recently, authors have reported novel designs of PCFs to achieve flat-gain performance in dual-concentric core [10] and W-type PCF structure [11] where the wavelength dependent effective area and leakage loss characteristics of the PCFs are utilized to achieve flat-Raman gain characteristics over the C-band. In contrary to the reported PCF designs, here we propose and investigate another new design of the PCF to attain more flat and wide-band Raman amplification over S-band. To accomplish better Raman performances

for the designed PCF, we have used genetic algorithm (GA) [11, 15] to optimize the PCF structural parameters. GA was combined with an efficient full-vectorial finite element modal (V-FEM) solver [16] based on the curvilinear edge/nodal hybrid elements with anisotropic perfectly matched layers.

In this paper, we have investigated Raman amplification properties of an optimized PCF in S-band using a single pump. The optimized PCF shows a very high negative dispersion coefficient (–264 ps/nm/km to –1410 ps/nm/km) and a negative dispersion slope over the range of operating wavelengths. Therefore, the proposed module comprised of 1.45-km long optimized PCF not only compensates for the dispersion accumulated in a span (80 km) of SSMF but also provides an average net gain of 1.65 dB with ±0.46 dB gain ripples over 50-nm bandwidth, high optical signal-to-noise ratio (OSNR), and low double Rayleigh backscattering (DRBS) values. Moreover, the designed PCF structure shows single mode behavior over the S-band. Hence, our designed module can act as a single-moded, broadband dispersion compensator and amplifier in a single unit for S-band.

The present study is organized as follows: In section 2, we introduce the topology of the optimized PCF structure and give a priori design guidelines to achieve the optimum design parameters. Then, in section 3, we briefly address Raman amplification model, which is well established and reported in many references. Numerical simulations and results are included in section 4, where we have obtained the dispersion characteristics and Raman performances of the proposed PCF. In section 5, we study the impact of fiber attenuation on the gain performances of the designed PCF. Then, in section 6, we carry out the fiber tolerance analysis, where we estimate the effect of each individual PCF design parameters on the performances of the device. In section 7, we conclude our investigations on the design of S-band dispersion compensating PCF Raman amplifiers.

2. Topology of PCF structure

Figure 1 depicts the transverse cross-section of the optimized PCF structure. The optimized PCF structure constitutes of three different air-hole diameters d (shown by white color filled circles), d' (shown by red color filled circles), and d'' (shown by yellow color filled circles) (shown in Fig. 1). The air-holes are regularly spaced in a hexagonal array with a lattice constant Λ. In the optimized structure, the ring core is built up at 6th air-hole ring by reducing the air-hole diameter to d' ($d > d'$). One can design the ring core freely after first air-hole ring depending on the desired dispersion characteristics. As the distance of the ring core increases from the fundamental core (i.e. inner core) the absolute magnitude of the dispersion increases. In our investigations, the ring core is built at 6th air-hole ring. The next two rings i.e. 7th and 8th possess the air-hole diameter same as of air-hole diameter of rings 1st to 5th (i.e. d). Further, the air-hole diameter of 9th to 13th rings is increased to d'' ($d'' > d > d'$) to ensure that the confinement loss remains below 0.1 dB/km level.

We have used GA to obtain the fiber structural parameters in such a way that the resulting PCF structure shows high negative dispersion in operating wavelength range and the modal field couples to the ring core after 1.52 μm wavelength, referred as phase matching wavelength (PMW). Physically, the PMW resembles the inflection point where the curvature changes from negative to positive or we can say that the fundamental super mode anti-crosses the individual core modes, causing the high negative dispersion at this point. To optimize the PCF parameters, following fitness function is defined

$$\begin{aligned} F\left(\Lambda, d, d^{'}\right) &= -\exp\left(w_1 f_1\right) \qquad \text{if } D(\lambda_1) > D(\lambda_2) > D(\lambda_3) \\ &= -1000 \qquad\qquad \text{else} \end{aligned} \tag{1}$$

with

$$f_1 = \sum_{\lambda=1.48\mu\text{m}}^{1.53\mu\text{m}} D\left(\lambda\right), \tag{2}$$

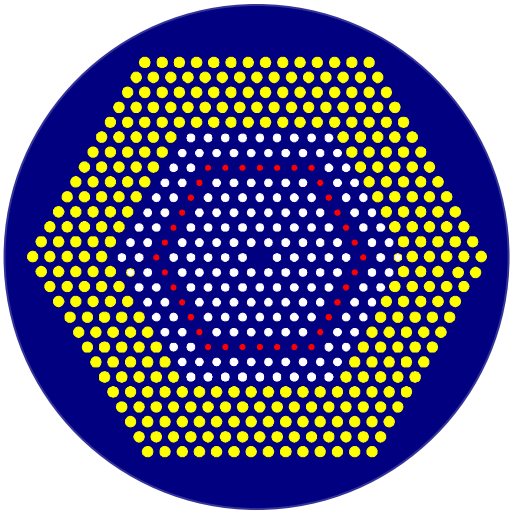

Fig. 1. Transverse cross-section of the optimized PCF structure having lattice constant Λ=1.375 μm, d/Λ = 0.4434 (1-5th and 7-8th air-hole rings, shown by white color filled circles), d'/Λ = 0.2962 (6th air-hole ring, shown by red color filled circles), and d''/Λ = 0.60 (9-13th air-hole rings, shown by yellow color filled circles).

where w_1 is the scaling parameter and is taken as 0.001, D is the chromatic dispersion coefficient in [ps/nm/km], and λ_1, λ_2, and λ_3 are 1.48 μm, 1.52 μm, and 1.53 μm wavelengths, respectively.

Clearly, the maximum value of fitness function F is zero when $w_1 f_1$ is $-\infty$. Therefore, maximizing F is equivalent to obtaining highly negative dispersion profile in the wavelength range of interest. An additional constraint as shown in Eq. (1) is imposed to ensure the monotonic decrement of the dispersion. Initial set of the structural parameters d, d', and Λ are defined within the practical range. After performing cross-over, mutation of structural parameters and after few generations, we get the optimized parameters as d/Λ = 0.4434, d'/Λ = 0.2962, Λ = 1.375 μm and the diameter of air-holes in outer ring d''/Λ = 0.60 is set manually as it doesn't affect the dispersion characteristics as well Raman performances (shown later) and keeps the leakage loss level below 0.1 dB/km.

To decide whether our PCF design is an optimum design or not, we have considered two different PCF design scenarios where the configuration of air-hole rings after the ring core is varied and their dispersion characteristics are noted. In first scenario, the diameter of the air-holes of air-hole rings 9-13 is assumed to be equal to the hole-diameter of the air-hole rings 1-5 and 7-8 i.e. $d''= d$. It is observed that this fiber design shows higher negative dispersion (shown by solid red curve in Fig. 2(a)) than the optimized fiber design with PMW shifted to short wavelengths but simultaneously exhibits large confinement loss (~600 dB/km). In second scenario, we consider the hole-diameter of air-hole rings 7-13 as d''. In the latter case, the dispersion shifts to upward direction (shown by solid black line) thus decreasing the absolute magnitude of the dispersion and extending the PMW to longer wavelengths. The dispersion characteristics of all three cases including the optimized fiber design and their corresponding confinement loss spectra are shown in Figs. 2(a) and (b). It can be clearly observed from the figures that for the optimized fiber design, a high negative dispersion characteristic (shown by solid blue curve) and very low confinement loss (shown by solid blue curve) are obtained. This analysis demonstrates that the design, shown in Fig. 1, is the optimum one to achieve the amplification over S-band with worthy dispersion characteristics.

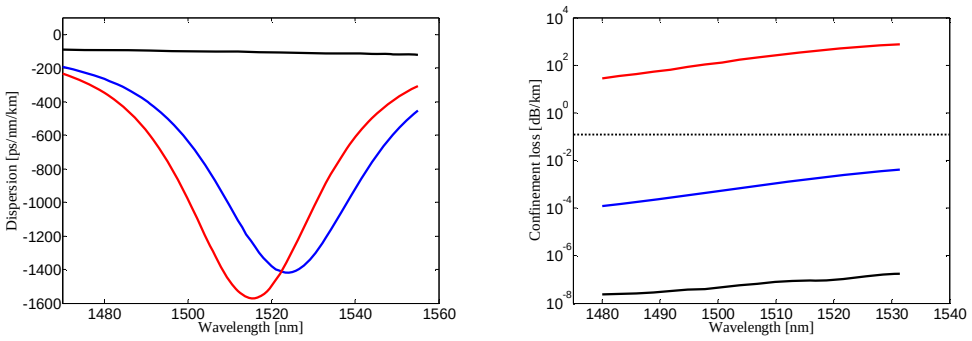

(a) (b)

Fig. 2. (a) Chromatic dispersion and (b) confinement loss of three different designed PCF structures; blue curve represents for the optimized fiber design as shown in Fig. 1, red curve denotes the case when the air-hole diameter of air-hole rings from 7 to 13 is d, while black curve stands for the case when the hole-diameter of air-hole rings 7-13 is d''.

Next, we establish the total number of rings by the following explanations. Firstly, we consider twelve numbers of total air-hole rings with distribution of air-hole rings such as two air-hole rings with hole-diameter d are placed after the ring-core (6th ring) and the rest four rings with d'' (i.e. 9-12th) constitutes outer core of the PCF structure. This structure consisting of total 12 number of air-hole rings provides the confinement loss above 0.1 dB/km level for longer wavelengths in S-band, which doesn't meet our requirement. Then, we consider a PCF design which has total thirteen number of air-hole rings that keeps the leakage loss below 0.1 dB/km. Therefore, from now onwards, we will consider the optimized fiber design (shown in Fig. 1) for investigating the Raman amplification properties. Additionally, the normalized frequency V-parameter [17] for the optimized PCF structure varies between 1.34 and 1.37 for S-band channels, which proves the single mode behavior of the designed PCF structure.

3. Raman Amplification model

After finding the set of optimized parameters for PCF as discussed in section 2, we obtain RGE γ_R, related to the frequency separation $\Delta\nu$ between the interacting signals [8, 18] as

$$\gamma_R = \iint_S C_{SiSi}(\Delta\nu) i_s(x,y) i_p(x,y)\, dxdy \tag{3}$$

where i_s and i_p are the normalized signal and pump intensities which are calculated through V-FEM by incorporating Poynting vector definition [8], S is the PCF cross-section, and $C_{SiSi}(\Delta\nu)$

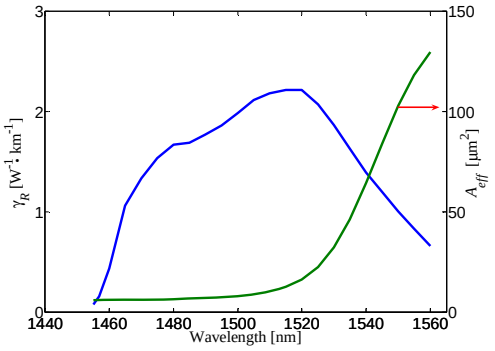

Fig. 3. Variation of RGE and effective area as a function of the wavelength. The RGE is obtained for an unpolarized light source at 1455-nm wavelength. The peak RGE value is 2.21 $W^{-1}\cdot km^{-1}$ at 1.52 μm.

is the Raman spectra relative to Si-O-Si bounds when the pump wavelength is λ_{ref}=1455-nm and given in [18]. The peak value of Raman gain coefficient for PCF (at $\Delta\nu$=13.2 THz), for unpolarized pump and signal, at 1455-nm pump wavelength is 3.34×10^{-14} m/W [8]. Figure 3 illustrates the variation of RGE and effective mode area as a function of the wavelength. It can be noticed from the Fig. 3 that the peak Raman gain value is 2.21 $W^{-1}\cdot km^{-1}$ at 1.52 μm wavelength. The effective area at 1.48, 1.51, and 1.53 μm wavelengths is 5.96, 10.36, and 32.12 μm^2, respectively. It is seen that the effective area increases sharply after 1.52 μm wavelength.

Next, a set of Raman propagation equations [11] which describe the interaction between pump and signals and consider the wavelength dependent fiber attenuation, amplified spontaneous emission (ASE), and Rayleigh backscattering, are solved numerically. Various Raman performances like net Raman gain, OSNR due to both ASE and Rayleigh backscattering, and noise figure (NF) are evaluated according to definitions in [11].

4. Numerical simulations and results

Figure 4(a) shows the variation of the chromatic dispersion of the optimized PCF and SSMF as a function of the wavelength. It can be clearly seen that for the optimized set of parameters and air-hole ring configurations, a large negative dispersion (−264 ps/nm/km to −1410 ps/nm/km) can be obtained which is monotonically decreasing over the S-band and possesses negative dispersion slope, providing fine dispersion compensation. Figure 4(b) corresponds to the residual dispersion obtained after the dispersion compensation by 1.45 km long PCF for the dispersion accumulated in one span (80 km) of SSMF. It can be observed that the residual dispersion is ±700 ps/nm, which is within the range of ±1000 ps/nm, enabling the proposed PCF structure to be suitable for 10 Gb/s transmission system [2].

Further, we consider 18 signal channels in S-band (202.70 THz-195.90 THz) spaced at 400 GHz, which propagate in the forward direction with an initial power of −10 dBm/ch. A single pump emitting 1450-nm wavelength with an input power of 520 mW is set to propagate in the contra-direction to the signals. Wavelength dependent fiber attenuation [19] spectrum is taken into account while solving the rate equations. In our calculations, we have considered fiber loss of 0.58 dB/km at 1550 nm wavelength [19]. Due to lack of experimentally measured fiber attenuation values of such PCF structures (except regular PCFs) we have evaluated the impact of fiber attenuation on the Raman performances of the device as shown in section 5. The net Raman gain spectrum obtained for 1.45-km long PCF is shown in Fig. 5 (a). The gain varies from minimum value of 1.1 dB to a maximum value of 2.1 dB with ±0.46 dB gain ripples over 50-nm bandwidth. To the best of our knowledge, it is the first wide-band gain-flattened amplification characteristics in PCFs.

DRBS is one of the major concerns in designing the FRAs as it can affect the noise performance of an amplifier. As the length of fiber increases, it becomes more pronounced. We have evaluated DRBS as a function of wavelength for the proposed structure and its variation is shown in Fig. 5(b). It can be observed that the optimized PCF shows a low DRBS value of −59.8 dB and on average DRBS value is −58.2 dB. Therefore, the DRBS will not affect the noise performance of the designed fiber amplifier module. The NF of the proposed fiber varies from 7.2 dB to 5.2 dB over S-band as shown in Fig. 5(c). The high value of NF at short wavelength is due to the pump depletion effect and the large fiber attenuation at pump wavelength. The OSNR (received at 0.1 nm bandwidth) spectrum for the designed module is depicted in Fig. 5(d). The module shows high OSNR value of 46.7 dB, while the average OSNR value is 44.8 dB over the range of operating wavelengths. The OSNR of 20 dB is the nominal level for all channels operated at BER $<10^{-12}$ without any correction at 10.67 Gb/s line rate [2]. Therefore our designed PCF is a suitable Raman gain media to provide amplification in S-band embedded with dispersion compensation functionality. Table 1 summarizes the Raman performances of the optimized PCF.

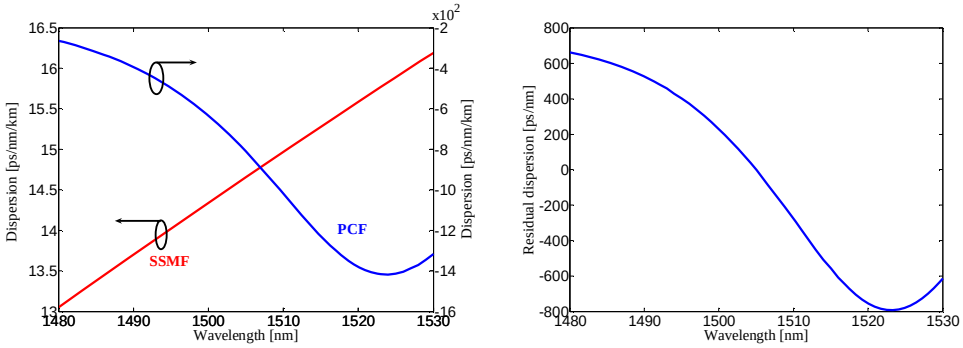

(a) (b)

Fig. 4. (a) Chromatic dispersion of the optimized PCF structure and SSMF. The dispersion for PCF lies between –264 ps/nm/km and –1410 ps/nm/km and (b) Residual dispersion after compensation of dispersion in one span (80-km) of SSMF link by 1.45-km long optimized PCF. The residual dispersion is ±700 ps/nm, thus enabling the proposed PCF to be a suitable for 10 Gb/s transmission networks.

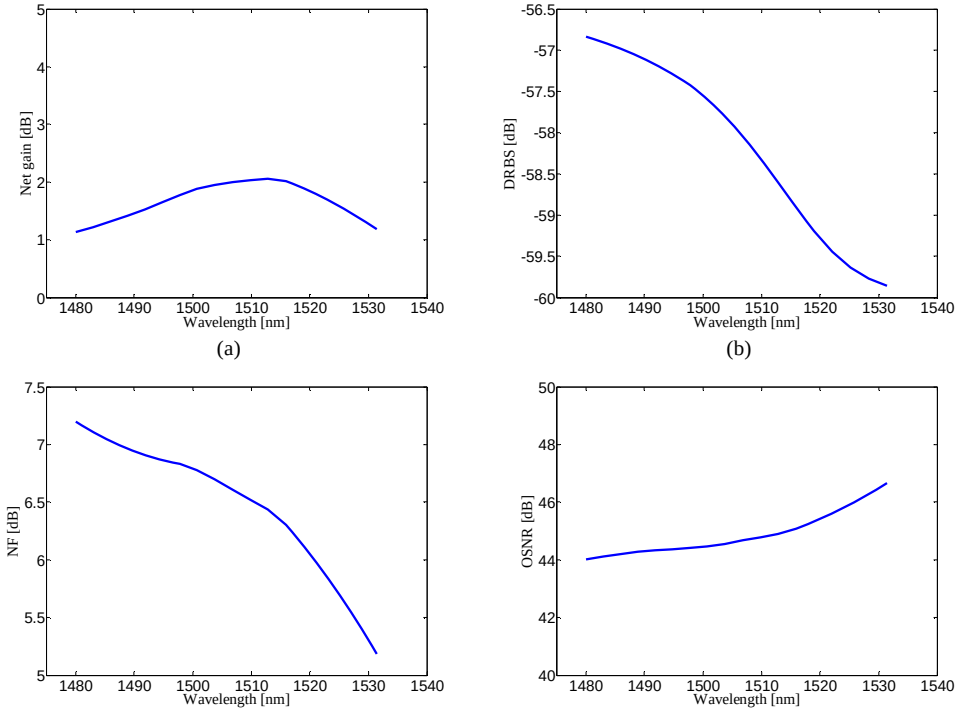

(a) (b)

(c) (d)

Fig. 5. Spectral variation of (a) net gain, (b) DRBS, (c) noise figure, and (d) optical signal-to-noise ratio for a single pump of 1450-nm and 18 S-band channels with an initial power of -10 dBm/ch in 1.45-km long optimized PCF.

Table 1. Raman performances of the optimized PCF (Λ=1.375 μm, d/Λ=0.4434, d'/Λ=0.2962, d''/Λ=0.60) for S-band.

Dispersion [ps/nm/km]	Length [km]	Average Net gain [dB]	Gain Ripples [dB]	Average OSNR [dB]	Average NF [dB]	Average DRBS [dB]
–(264-1410)	1.45	1.65	±0.46	44.8	6.5	–58.2

5. Impact of fiber attenuation

Due to lack of experimental data for fiber attenuation for such complex PCF geometry, we consider the affect of fiber attenuation on the Raman performances especially on the net gain of the optimized PCF. It may expect that the optimized PCF configuration may possess high attenuation values of few dB/km.

To note the influence of the fiber loss on the gain features, we start with the fiber attenuation spectrum of a regular PCF as mentioned in [20], where the PCF shows the lowest attenuation of 0.37 dB/km at 1.55 μm wavelength. We then raise the absolute magnitude of the attenuation to different loss levels keeping constant its spectral variation. The net gain obtained for different fiber attenuation levels of 10 dB/km, 5 dB/km, 0.58 dB/km [19], and 0.37 dB/km is plotted in Fig. 6 as a function of the wavelength and attenuation as a parameter. It can be seen from Fig. 6 that for highest attenuation of 10 dB/km, the fiber doesn't provide any gain to the signal and solely acts as a dispersion compensator only. As the attenuation decreases, the signals receive the gain. Therefore, we expect that with the development of fabrication technologies in near future, the losses of such complex PCF structures can be reduced to the level of conventional high delta fiber (0.55 dB/km @ 1.55 μm).

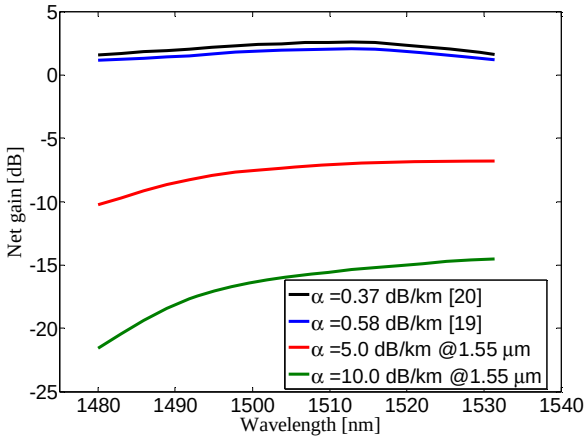

Fig. 6. Variation of net gain as a function of wavelength with fiber attenuation as a parameter.

6. Tolerance analysis for dispersion and Raman amplification properties

In the view of the practical feasibility and compatibility of our proposed device, the fiber tolerance may occur up to 1% [21, 22]. In this section, we have performed the sensitivity analysis of each an individual PCF design parameter within a tolerance of ±1%. Tolerance impact is observed for the performances of the proposed PCF Raman amplifier module in terms of its dispersion and gain characteristics.

6.1 Effect of lattice constant

The lattice constant is varied by ±1% to its optimum value while keeping other fiber parameters fixed. The influence of pitch tolerance is noted for the fiber's chromatic dispersion and gain characteristics. Figures 7(a) and (b) correspond to the dispersion and net gain spectra. Red and black color solid curves dictate the variation in the pitch by +1% and −1%, respectively, while the blue color solid curve presents the optimum design characteristics. It can be examined that the dispersion shifts to up/down direction with increase/decrease in the pitch value, while the gain decreases/increases with increase/decrease of the pitch constant. For example, for 1% increment/decrement of the pitch, the gain decreases/increases to an average value of 1.5 dB/1.7 dB while the average gain for the optimized PCF is 1.65 dB. The increment/decrement in the gain values comes from the strong/weak overlap between pump and signal modal field intensities as there is very slight shift of the PMW, which determines the strength of the overlap between the pump and signals. It can be concluded that ±1% change in the lattice constant doesn't affect the performances of the device drastically.

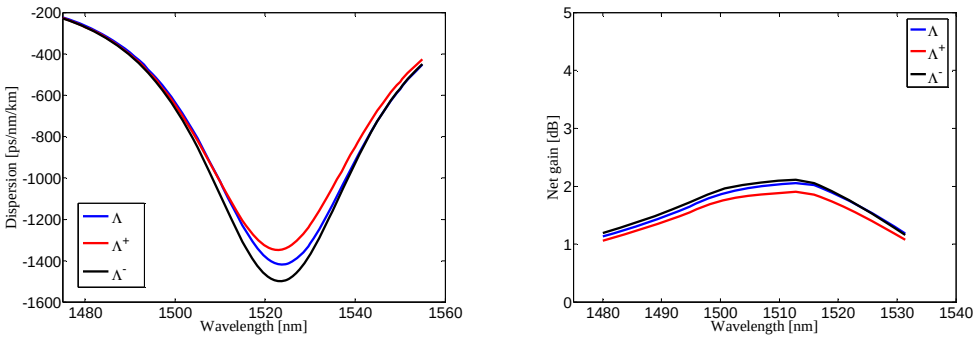

(a) (b)

Fig. 7. (a) Dispersion and (b) net gain characteristics of the optimized PCF with a tolerance of ±1% in the lattice constant. Red and black color solid lines represent the variation of lattice constant by ±1%, while blue color solid line stands for the optimized PCF structure.

6.2 Variation of hole-diameter of inner five rings (1-5)

As a next step, we fix the lattice constant, hole-diameter of ring core (*d'*), hole-diameter of outer air-hole rings (*d''*) and vary the hole-diameter *d* of the first five air-hole rings. One percent change in the diameter of air-holes alters the dispersion properties of the optimized PCF. The absolute magnitude of the dispersion coefficient increases and the PMW shifts to shorter wavelengths for 1% increment in *d*, while 1% decrement in *d* results into the shift of the dispersion coefficient to positive direction and PMW to longer wavelength, as shown in Fig. 8(a). The shift of PMW to shorter and longer wavelength produces weak and strong coupling of pump and signal modal field intensities and thus causes the Raman gain to decrease and increase accordingly as shown in Fig. 8(b). The maximum net gain changes to 1.1 dB or 3.51 dB from 2.1 dB level (corresponding to blue line) for 1% increment or decrement of the hole-diameter *d*. Therefore, it can be concluded that almost 1 dB variation is observed for 1% tolerance in the hole-diameter of first five air-hole rings.

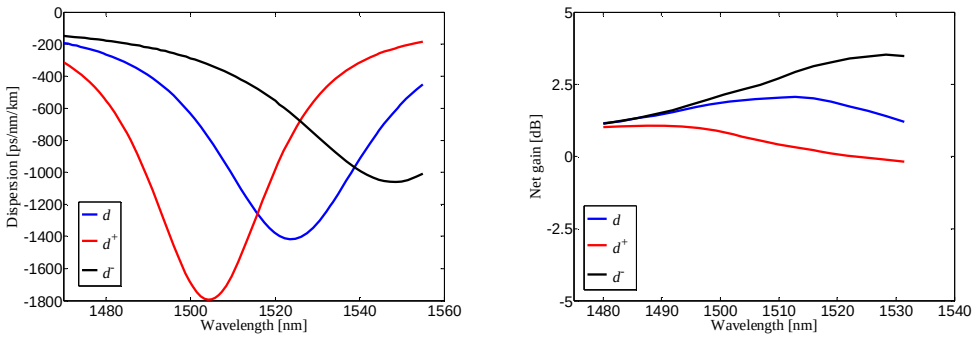

(a) (b)

Fig. 8. (a) Dispersion and (b) net gain characteristics of the optimized PCF with a tolerance of ±1% in the hole-diameter *d* of first five air-hole rings while keeping other design parameters fixed. Red and black color solid lines represent the variation of hole-diameter *d* of first five air-hole rings by ±1%, while blue color solid line stands for the optimized PCF structure.

6.3 Influence of hole-diameter of the ring-core (6)

To analyze the impact of the fiber tolerance in the hole-diameter of the air-holes of ring core (6th air-hole ring), we vary the hole-diameter *d′* of the air-holes in ring-core by ±1% to its optimum value and while we fix other fiber parameters in their optimum values as stated before. Figure 9(a) plots the dispersion characteristics of the PCF and presents the shift in the dispersion curves from the optimum one (solid blue curve). It is seen that the minima of the dispersion curves shift to shorter and longer wavelengths for decrement and increment of 1% change in hole-diameter *d′* opposite to features observed in section 6.2. This shift mainly occurs due to the variation in PMW. Figure 9(b) corresponds to the variation of the net gain as a function of the signal wavelengths for ±1% change in *d′*. It can be clearly seen that the net gain increases to 3.4 dB level for 1% increase in *d′* (solid red curve), while the net gain decreases to 0.8 dB value for 1% decrease in *d′* (solid black curve). When *d′* increases by 1%, the PMW get shifted to longer wavelength and hence the overlap between the pump and signal modal field intensities become stronger, causing higher gain. Similarly, the strength of the overlap between pump and signals become weaker for 1% decrease in *d′* due to shift of PMW to short wavelengths, giving lower values of the gain with respect to the gain corresponding for the optimum design parameters (solid blue curve).

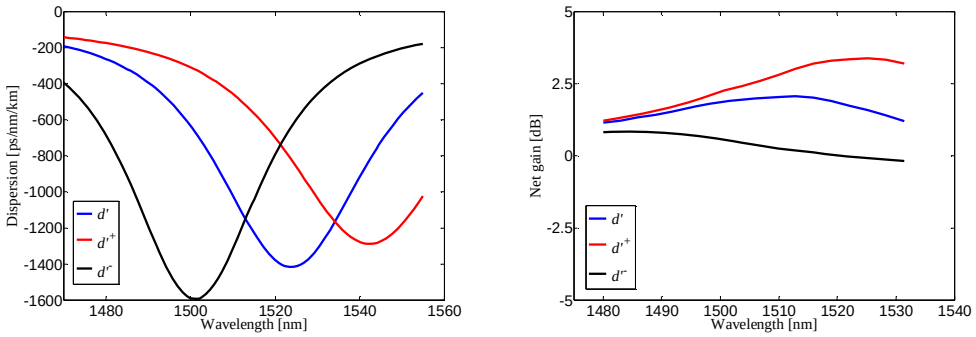

(a) (b)

Fig. 9. (a) Dispersion and (b) net gain characteristics of the optimized PCF with a tolerance of ±1% in the hole-diameter *d′* of ring-core (i.e. 6th air-hole ring) while keeping other design parameters fixed. Red and black color solid curves represent the variation of hole-diameter *d′* of ring-core by ±1%, while blue color solid curve stands for the optimized PCF structure.

6.4 Variation of hole-diameter of air-hole rings 7 and 8

Next, if we vary the hole-diameter of the air-holes in seventh and eighth air-hole rings by ±1% to its optimum value, the dispersion and net gain characteristics alters accordingly as shown in Figs. 10(a) and (b). It can be interpreted from the figures that the change of ±1% in the hole-diameter of the 7th and 8th air-hole rings resembles like to the variation of hole-diameter of the air-holes in the ring-core (shown in Figs. 9(a) and (b)). One can conclude that the 7th and 8th air-hole rings effectively behave as a ring-core.

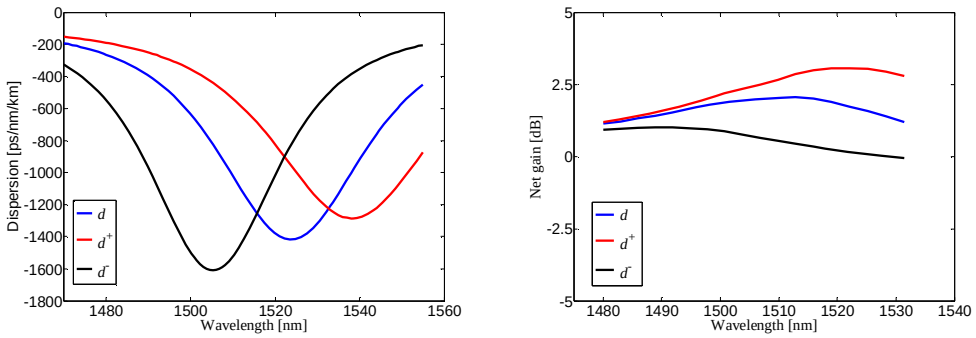

(a) (b)

Fig. 10. (a) Dispersion and (b) net gain characteristics of the optimized PCF with a tolerance of ±1% in the hole-diameter *d* of the 7th and 8th air-hole rings while keeping other design parameters fixed. Red and black color solid curves represent the variation of hole-diameter *d* of the 7th and 8th air-hole rings by ±1%, while blue color solid curve stands for the optimized PCF structure.

6.5 Effect of varying the hole-diameter of outer air-hole rings (9-13)

Finally, we study the influence of 1% tolerance in the outer air-hole rings (9-13 air-hole rings). The hole-diameter *d″* of the air-holes in 9th-13th air-hole rings is varied by ±1% to its optimum value and the impact of this variation on fiber chromatic dispersion and net gain properties is plotted in Figs. 11(a) and (b). It can be concluded from the figures that the neither the dispersion nor the net gain characteristics change so much. The change in dispersion and gain remains below 1% to the values obtained for the optimum fiber design parameters. Therefore, it can be concluded that the tolerances of 1% in the outer air-holes don't affect the performance of the proposed device.

From the above thorough and detailed investigations of the impact of fiber tolerances on the performances of the proposed PCF Raman amplifier module operating in S-band, it can be concluded that the tolerances should be kept below 1% for the successful operation of the device. Further, we would like to add comments in support of the practicality of the proposed PCF Raman amplifier module. The splicing of PCFs with SSMFs has been made possible as mentioned in [23] where a splice loss of 0.6 dB between SSMF and highly nonlinear PCF was observed experimentally. Hence, we expect that the proposed PCF can be interfaced with existing technology with no added complications. Fabrication of complex designed PCF is one of the important issues. PCFs with depressed inner cladding with 8-10 numbers of air-hole rings have been fabricated successfully [21, 22] and their dispersion characteristics are measured experimentally. Therefore, by adopting such fabrication technologies, our proposed PCF design can be fabricated keeping the tolerances below 1% especially in the diameter of air-holes in surrounding the inner core. The Raman performances of the proposed PCF module in terms of length, gain, OSNR, DRBS, NF, and overall dispersion characteristics are far better than the Raman performances of the FRA based on conventional optical fiber as mentioned in [5].

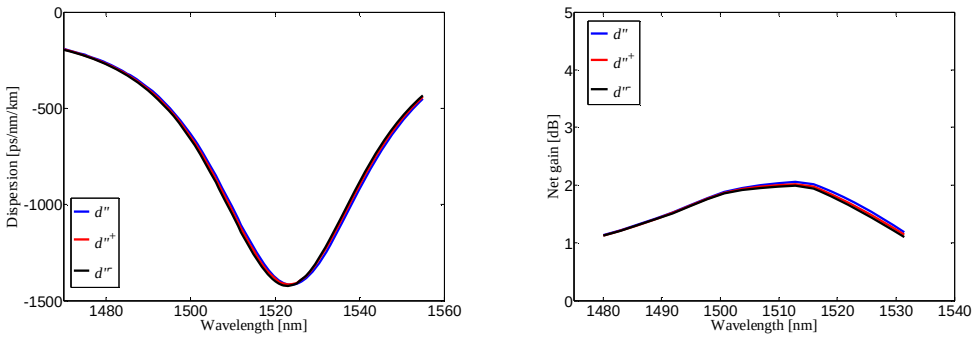

(a) (b)

Fig. 11. (a) Dispersion and (b) net gain characteristics of the optimized PCF with a tolerance of ±1% in the hole-diameter d'' of 9-13th air-hole rings while keeping other design parameters fixed. Red and black color solid curves represent the variation of hole-diameter d'' of 9-13th air-hole rings by ±1%, while blue color solid curve stands for the optimized PCF structure.

At the end, we summarize the impact of fiber tolerances on Raman performances of the proposed fiber in Table 2. It can be inferred from Table 2 that ±1% change in the hole-diameter of air-holes of the ring core may affect the gain ripples of the module while other properties such as avg. (average) OSNR, avg. DRBS, and avg. NF changes by less than 1%. It can be estimated from the Table 2 that avg. OSNR, DRBS, and NF don't shift from their nominal values largely for ±1% variation in pitch, hole-diameter of 1st to 5th ($d_{1\text{-}5}$) air-hole rings, hole-diameter of ring core (d_6), hole-diameter of 7th-8th ($d_{7\text{-}8}$) air-hole rings, and hole-diameter of 9th-13th ($d_{9\text{-}13}$) air-hole rings. Here, we would like to emphasis that our proposed device shows better Raman performances than the reported one in Ref. [5].

Table 2. Impact of the fiber tolerances on the Raman performances of the proposed PCF module.

	Optim.	Variation of +1% in					Variation of –1% in				
		Λ	$d_{1\text{-}5}$	d_6	$d_{7\text{-}8}$	$d_{9\text{-}13}$	Λ	$d_{1\text{-}5}$	d_6	$d_{7\text{-}8}$	$d_{9\text{-}13}$
Gain ripple [dB]	±0.46	±0.48	±0.62	±1.1	±0.94	±0.45	±0.42	±1.2	±0.51	±0.53	±0.44
Avg. OSNR [dB]	44.8	44.8	46.8	49.2	44.3	44.9	45.0	44.2	47.2	46.7	44.9
Avg. DRBS [dB]	–58.2	–58.1	–59.1	–57.1	–57.4	–58.2	–58.3	–57.2	–59.3	–59.1	–58.2
Avg. NF [dB]	6.4	6.5	5.2	7.0	6.9	6.5	6.4	6.9	4.9	5.3	6.4

7. Summary

To summarize our work, we have investigated the Raman amplification properties of the newly designed and optimized PCF structure over S-band using a single pump for the first time. The fiber is designed such that it exhibits high negative dispersion coefficient (–264 ps/nm/km to –1410 ps/nm/km) with a negative dispersion slope, enabling coarse dispersion compensation over the range of operating wavelengths. To evaluate flat-gain characteristics,

the PCF structural parameters are optimized by combining the GA and V-FEM. Wide-band Raman amplification with gain ripples of ±0.46 dB over 50 nm is successfully achieved using a single pump and an average low DRBS value (−58.2 dB) is obtained along with high OSNR values up to 46.7 dB. The proposed module comprised of 1.45 km long PCF can compensate for the dispersion accumulated in one span (80 km) of SSMF with a residual dispersion of ±700 ps/nm, which suggests the applicability of investigated PCF for 10 Gb/s WDM transmission system. Next, we have carried out the effect of fiber attenuation on Raman performances of the optimized PCF and it was observed that module solely acts as a dispersion compensator for high attenuation values. Further, we have performed the tolerance analysis for each individual fiber design parameters. It was examined that ±1% disorder in the hole-diameter of air-hole rings affects the dispersion properties drastically but the Raman gain changes to 10% of its nominal value. Therefore, for the successful and practical operation of the device, the fiber tolerances should be kept below ±1%. Additionally, the optimized PCF remains single mode over the range of operating wavelength, which is one of the solid aspects of the PCF over conventional fibers.

Acknowledgements

Authors acknowledges to 21st Century COE (Center of Excellence) program: Meme-Media Technology Approach to the R&D of the Next Generation Information Technologies.